

## Modification of Exponential Based Hyperelastic Strain Energy to Consider Free Stress Initial Configuration and Constitutive Modeling

Milad Arman<sup>a</sup>, Keivan Narooei<sup>a</sup> \*

<sup>a</sup> Department of Materials Science and Engineering, K. N. Toosi University of Technology, Tehran, Iran.

### ARTICLE INFO

#### Article history:

Received: 03 November 2017

Accepted: 26 January 2018

#### Keywords:

Hyperelastic

Natural rubber

Thermoplastic elastomer

Unstressed configuration

VUMAT

Stability

### ABSTRACT

In this research, the exponential stretched based hyperelastic strain energy was modified to provide the unstressed initial configuration. To this end, as the first step, the model was calibrated by the experimental data to find the best material parameters. The fitting results indicated material stability in large deformations and basic loading modes. In the second step, the initial pseudo stress value (ISV) was eliminated from the hyperelastic strain energy using a function of the determinant of the deformation gradient. The modified and unmodified models were implemented in ABAQUS/VUMAT user subroutine and the deformation behavior of the natural rubber and the thermoplastic elastomer was predicted. The results obtained from the modified model represented a better agreement with the experimental data, in comparison to those gained by the unmodified model. In order to present the significance of the unstressed initial configuration in engineering applications, the stenting phenomenon in the atherosclerosis human artery was investigated. It was revealed that a uniform stress distribution could be achieved in the artery using the modified model, thereby reducing the possibility of tearing and restenosis.

### 1. Introduction

Hyperelastic strain energy functions are used to predict the nonlinear elastic deformation of soft tissues, nanomaterials, and elastomeric materials in large deformations [1]. However, it is important to choose an appropriate hyperelastic strain energy function and determine material parameters from the available mechanical tests.

In the recent years, many researchers have studied the nonlinear elastic deformation of materials using the experimental and theoretical methods. For example, Sasso et al studied the mechanical response of the rubber-like materials using hyperelastic models, concluding that the Ogden model could provide a good prediction in the finite element (FE) simulations [2]. Casem et al studied the strain rate and the specimen size effects on the mechanical behavior of the thermoplastic elastomer gel tissue in the uniaxial compression test [3]. The experimental results showed the strain rate sensitivity, while the FE simulations illustrated good results only in the low strain rates. Li et al studied the effects of size and rubber content on the mechanical behavior (strength, elastic modulus and failure) of

concrete using the uniaxial compression test [4]. Li et al investigated the nonlinear elastic behavior of natural rubbers (NR) using the modified Arruda-Boice hyperelastic model, observing a relatively good agreement with the experimental results [5]. Shergold et al measured the mechanical response of the pig skin and silicon rubber under uniaxial compression in wide strain rate ranges [6]. The numerical results showed that the Mooney-Rivlin model did not fit the uniaxial compression test data very well. Beda and Chevalier generalized the Ogden hyperelastic model in terms of two invariants to study the mechanical response of rubber-like materials [7]. Further, Beda presented a new mathematical strategy to build proper hyperelastic models without considering initial stresses and accordingly proposed a new function based on the Hart-Smith model [8]. Ogden et al investigated the mechanical behavior of incompressible rubber materials and found the optimized material parameters using the nonlinear least square algorithm [9]. Terada et al proposed a new strategy to take into account the mechanical response of fiber-reinforced materials based on hyperelastic models [10]. Gendy and Saleeb combined the optimization and sensitivity analysis to estimate the material parameters of

\* Corresponding author. Tel.: +98-21-84063283; fax: +98-21-88785238; e-mail: [knarooei@kntu.ac.ir](mailto:knarooei@kntu.ac.ir)

hyperelastic functions on the rubbers and foam-like materials more accurately [11]. Drozdov presented a novel hyperelastic model based on the thermodynamics of polymer networks, and accurate results were achieved in the uniaxial tension, uniaxial compression, simple shear, and pure shear loadings [12]. Darijani et al developed the Saint-Venant Kirchhoff hyperelastic model for isotropic materials, concluding that their model exhibited a good agreement with the experimental data [13]. Darijani and Naghdabadi proposed new hyperelastic functions based on the logarithmic, exponential, power, and polynomial functions, verifying that the suggested models could predict the experimental data reasonably [14]. Mansouri and Darijani proposed the general exponential hyperelastic model based on the generalization of the previous research and investigated the response of elastomers and the porcine liver tissue [15]. Accordingly, Fereidoonzhad et al proposed a two-part hyperelastic model (isotropic and anisotropic) to predict the mechanical behavior of transversely isotropic materials [16]. To the best of our knowledge, the effect of pseudo initial stresses in the constitutive modeling of general loading has not yet been considered.

One of the main purposes of the hyperelastic models development is to simulate and optimize the biological phenomena. To this goal, many researchers have investigated the mechanical behavior of tissues such as brain, bone, and muscles, as well as their performance in body, by using FE analysis [17-19]. Nonetheless, due to the significance of the coronary artery disease (CAD), many studies have been focused on the mechanical response of the arteries by considering the material and geometry of the coronary and stent [20-22]. For example, Prendergast et al considered the uniaxial and biaxial tension tests on the human and porcine artery using a polynomial hyperelastic model for the stenting process [23]. Karimi et al investigated the linear mechanical properties of the abdominal vein and artery [24]. The results demonstrated that both Ogden and Mooney-Rivlin models fitted the vein experimental data, and the Ogden model captured the artery experimental data. Holzapfel et al performed the uniaxial tension test on several layers of non-atherosclerosis arteries and estimated the material parameters of a polynomial anisotropic-hyperelastic model [25]. However, the predicted results did not fit appropriately the experimental curves. Imani et al considered the five-term Mooney-Rivlin model to simulate the artery deformation due to the Multi-Link and Palmaz-Schatz stents expansion, obtaining the stress distribution and the outer diameter changes of the human artery [26]. Eshghi et al assumed the polynomial hyperelastic model for the human artery and evaluated the stress distribution, the bending of the stent, and the outer diameter changes during the stent deployment [27].

Based on the above literature review, the significance of hyperelastic modeling can be conceived in different engineering applications. Recently, an exponential based hyperelastic model as a function of stretches has been proposed by Mansouri and Darijani [15]. In the current research, this model was modified to consider the initial zero stress in the undeformed (unstressed) configuration for the simulations of general loading. To explain the significance of modification in the engineering applications, the uniaxial tension of the natural rubber, the uniaxial compression of the thermoplastic elastomer, and atherosclerosis artery deformation during stenting were investigated using the VUMAT user subroutine. Based on these descriptions, in the next sections, first the hyperelastic model is introduced. Then, the zero stress modification of the hyperelastic strain energy and constitutive modeling are described. Finally, the results of simulations are compared with those obtained by other researchers.

## 2. Hyperelastic material constants determination

Mooney-Rivlin and Ogden hyperelastic strain energy functions are the most famous constitutive models widely used in researches [28, 29]. However, these hyperelastic models generally cannot properly accommodate different deformations. Therefore, Mansouri and Darijani proposed a general hyperelastic strain energy in the exponential framework as [15]:

$$W = \sum_{i=1}^{\infty} A_i \left[ e^{m_i (\lambda_1^{\alpha_i} + \lambda_2^{\alpha_i} + \lambda_3^{\alpha_i} - 3)} - 1 \right] + \sum_{l=1}^{\infty} B_l \left[ e^{n_l (\lambda_1^{-\beta_l} + \lambda_2^{-\beta_l} + \lambda_3^{-\beta_l} - 3)} - 1 \right] \quad (1)$$

where  $A_k$ ,  $B_k$ ,  $m_k$ ,  $n_k$ ,  $\alpha_k$ , and  $\beta_k$  are the material constants found by fitting to the experimental data, and  $\lambda_i$  refers to the principal stretches. They showed that the proposed model could predict the stress response of different materials like rubbers and biomaterials in basic deformation modes. The principal second Piola-Kirchhoff stress components ( $S_i$ ) can be calculated from the hyperelastic strain energy as [29]:

$$S_i = \frac{1}{\lambda_i} \frac{\partial W}{\partial \lambda_i} \quad (\text{no sum on repeated indices}) \quad (2)$$

To determine the material parameters, the relative error ( $RE$ ) between the theoretical and experimental data can be defined as:

$$RE(\%) = \frac{\|S^{theo}(\lambda) - S^{exp}(\lambda)\|_{L_2}}{\|S^{exp}(\lambda)\|_{L_2}} \times 100 \quad (3)$$

where  $S^{theo}$  and  $S^{exp}$  represent the theoretical and experimental stresses as a function of the principal stretches respectively. The symbol  $\| \cdot \|_{L_2}$  in Eq. 3 shows the  $L_2$  norm. By minimizing the relative error ( $RE$ ), the material parameters can be defined. It is worth mentioning that the experimental stresses are in Lagrangian (nominal) or Cauchy (real) stress measures, and an appropriate transformation to the second Piola-Kirchhoff stress should be considered by the well-known transformations of continuum mechanic's rules [29, 30].

## 3. Initial stress Modification and Constitutive modeling

Finite element modeling of the mechanical response of materials needs to find an appropriate constitutive model. The hyperelastic models used in commercial finite element software cannot generally consider the mechanical behavior of all materials. Therefore, it is usually needed to implement new constitutive equations via the user material subroutines. In the ABAQUS software, constitutive modeling can be performed using VUMAT or UMAT user subroutines. In this research, the VUMAT user subroutine was used, because the contact problem of stenting could be simulated more efficiently via the ABAQUS/Explicit solver. In simple loading cases (like uniaxial tension), the undetermined incompressibility parameter can be defined via the zero stress conditions in specific directions (for example transverse directions in uniaxial tension). Nevertheless, in general loading cases the incompressibility constraint should be imposed via Lagrange multipliers or penalty methods. As the Lagrange multipliers method needs the linearization of hyperelastic models and increase the computational time, this method is seldom used. The incompressibility condition can be imposed on Eq. 1 by penalty method as a function of the determinant of the deformation gradient ( $J$ ) [31]:

$$W = \sum_{i=1}^{\infty} A_i \left[ e^{m_i (\lambda_1^{\alpha_i} + \lambda_2^{\alpha_i} + \lambda_3^{\alpha_i} - 3)} - 1 \right] + \sum_{l=1}^{\infty} B_l \left[ e^{n_l (\lambda_1^{-\beta_l} + \lambda_2^{-\beta_l} + \lambda_3^{-\beta_l} - 3)} - 1 \right] + \frac{1}{K} (J - 1)^2 \quad (4)$$

In this equation,  $K$  is a small number employed to impose the incompressibility condition. By using Eqs. 2 and 4, the stress components in the principal stress space can be derived as:

$$\begin{aligned} S_1 &= \sum_{i=1}^{\infty} A_i m_i \alpha_i \lambda_1^{\alpha_i - 2} e^{m_i (\lambda_1^{\alpha_i} + \lambda_2^{\alpha_i} + \lambda_3^{\alpha_i} - 3)} \\ &\quad - \sum_{l=1}^{\infty} B_l n_l \beta_l \lambda_1^{-\beta_l - 2} e^{n_l (\lambda_1^{-\beta_l} + \lambda_2^{-\beta_l} + \lambda_3^{-\beta_l} - 3)} + \frac{2}{K} (\lambda_1 \lambda_2 \lambda_3 - 1) \frac{\lambda_2 \lambda_3}{\lambda_1} \\ S_2 &= \sum_{i=1}^{\infty} A_i m_i \alpha_i \lambda_2^{\alpha_i - 2} e^{m_i (\lambda_1^{\alpha_i} + \lambda_2^{\alpha_i} + \lambda_3^{\alpha_i} - 3)} \\ &\quad - \sum_{l=1}^{\infty} B_l n_l \beta_l \lambda_2^{-\beta_l - 2} e^{n_l (\lambda_1^{-\beta_l} + \lambda_2^{-\beta_l} + \lambda_3^{-\beta_l} - 3)} + \frac{2}{K} (\lambda_1 \lambda_2 \lambda_3 - 1) \frac{\lambda_1 \lambda_3}{\lambda_2} \\ S_3 &= \sum_{i=1}^{\infty} A_i m_i \alpha_i \lambda_3^{\alpha_i - 2} e^{m_i (\lambda_1^{\alpha_i} + \lambda_2^{\alpha_i} + \lambda_3^{\alpha_i} - 3)} \\ &\quad - \sum_{l=1}^{\infty} B_l n_l \beta_l \lambda_3^{-\beta_l - 2} e^{n_l (\lambda_1^{-\beta_l} + \lambda_2^{-\beta_l} + \lambda_3^{-\beta_l} - 3)} + \frac{2}{K} (\lambda_1 \lambda_2 \lambda_3 - 1) \frac{\lambda_1 \lambda_2}{\lambda_3} \end{aligned} \quad (5)$$

According to the hyperelasticity conditions [14], the stress tensor should be zero at the undeformed configuration (initial configuration). Therefore, by substituting the undeformed configuration ( $\lambda_1 = \lambda_2 = \lambda_3 = 1$ ) in Eq. 5, the initial stress value (ISV) can be expressed as:

$$ISV = \sum_{i=1}^{\infty} A_i \alpha_i m_i - \sum_{l=1}^{\infty} B_l \beta_l n_l \quad (6)$$

It should be noted that in the case of the large value of material parameters, ISV could influence the computed stresses considerably. Now, to eliminate the spurious initial stress, Eq. 4 could be modified by subtracting ISV as a function of  $(J - 1)$ , as follows:

$$W = \sum_{i=1}^{\infty} A_i \left[ e^{m_i (\lambda_1^{\alpha_i} + \lambda_2^{\alpha_i} + \lambda_3^{\alpha_i} - 3)} - 1 \right] + \sum_{l=1}^{\infty} B_l \left[ e^{n_l (\lambda_1^{-\beta_l} + \lambda_2^{-\beta_l} + \lambda_3^{-\beta_l} - 3)} - 1 \right] + \frac{1}{K} (J - 1)^2 - (ISV)(J - 1)^2 \quad (7)$$

Indeed, in Eq. 7, the last term is imposed on the strain energy function as a constraint to deliver zero stress on the initial configuration[29]. By assuming Eqs. 2 and 7, the stress components can be obtained as (assuming one term in the summation of Eqs. 4 or 7):

$$\begin{aligned} S_1 &= A_1 m_1 \lambda_1^{\alpha_1 - 2} \alpha_1 e^{m_1 (\lambda_1^{\alpha_1} + \lambda_2^{\alpha_1} + \lambda_3^{\alpha_1} - 3)} - B_1 n_1 \lambda_1^{-\beta_1 - 2} \beta_1 e^{n_1 (\lambda_1^{-\beta_1} + \lambda_2^{-\beta_1} + \lambda_3^{-\beta_1} - 3)} + \\ &\quad \frac{2}{K} (\lambda_1 \lambda_2 \lambda_3 - 1) \frac{\lambda_2 \lambda_3}{\lambda_1} - (A_1 \alpha_1 m_1 - B_1 \beta_1 n_1) \frac{\lambda_2 \lambda_3}{\lambda_1} \\ S_2 &= A_1 m_1 \lambda_2^{\alpha_1 - 2} \alpha_1 e^{m_1 (\lambda_1^{\alpha_1} + \lambda_2^{\alpha_1} + \lambda_3^{\alpha_1} - 3)} - B_1 n_1 \lambda_2^{-\beta_1 - 2} \beta_1 e^{n_1 (\lambda_1^{-\beta_1} + \lambda_2^{-\beta_1} + \lambda_3^{-\beta_1} - 3)} + \\ &\quad \frac{2}{K} (\lambda_1 \lambda_2 \lambda_3 - 1) \frac{\lambda_1 \lambda_3}{\lambda_2} - (A_1 \alpha_1 m_1 - B_1 \beta_1 n_1) \frac{\lambda_1 \lambda_3}{\lambda_2} \\ S_3 &= A_1 m_1 \lambda_3^{\alpha_1 - 2} \alpha_1 e^{m_1 (\lambda_1^{\alpha_1} + \lambda_2^{\alpha_1} + \lambda_3^{\alpha_1} - 3)} - B_1 n_1 \lambda_3^{-\beta_1 - 2} \beta_1 e^{n_1 (\lambda_1^{-\beta_1} + \lambda_2^{-\beta_1} + \lambda_3^{-\beta_1} - 3)} + \end{aligned}$$

$$\frac{2}{K} (\lambda_1 \lambda_2 \lambda_3 - 1) \frac{\lambda_1 \lambda_2}{\lambda_3} - (A_1 \alpha_1 m_1 - B_1 \beta_1 n_1) \frac{\lambda_1 \lambda_2}{\lambda_3} \quad (8)$$

In the VUMAT user subroutine, the right stretch tensor in each increment has been provided in the current configuration. So, the eigenvectors and eigenvalues of the right stretch tensor were obtained by VSPRIND utility routines. By using Eq. 8, the principal second Piola-Kirchhoff stress components were computed according to the principal values of the right stretch tensor. Finally, to calculate the second Piola-Kirchhoff stress in the current configuration, the following transformation was used [32]:

$$S = S_1 N_1 \otimes N_1 + S_2 N_2 \otimes N_2 + S_3 N_3 \otimes N_3 \quad (9)$$

where  $N_1$ ,  $N_2$ , and  $N_3$  are the right stretch tensor eigenvectors. It is worth mentioning that in the VUMAT user subroutine, the corotational Cauchy stress ( $\hat{\sigma}$ ) should be updated in each increment as [32, 33]:

$$\hat{\sigma} = \frac{1}{J} USU^T \quad (10)$$

where  $U$  is the stretch tensor and  $S$  represents the second Piola-Kirchhoff stress tensor.

#### 4. Results and Discussion

In this section, first, the material parameters derived from experimental data are presented. Then, the results of the simulation of the uniaxial tension of the natural rubber, the uniaxial compression of the thermoplastic elastomer, and the stenting of atherosclerosis artery are discussed.

##### 4.1. Material parameters evaluation

Generally, the strain energy functions should be calibrated by the experimental data. In this paper, the experimental data (uniaxial and equi-biaxial tension tests) of atherosclerosis coronary artery were adopted from Prendergast et al [23], and the natural rubber uniaxial tension test data were provided from Li et al [5]. To investigate the compressive behavior, the uniaxial compression data of thermoplastic elastomer (TPE) at the strain rate of 0.01/s was extracted from Casem et al [3]. By using the nonlinear least square method and selecting the initial value for fitting parameters between zero and one, the experimental data were fitted to the exponential based hyperelastic strain energy function (Eq. 1) and the best material parameters were determined. Table 1 represents the material parameters and Fig .1 shows the experimental and fitted curves. It should be noted that the equi-biaxial and pure shear experimental data were not available for the natural rubber and thermoplastic elastomer. However, the shear and equi-biaxial stresses were plotted to check the material stability in these loading conditions.

**Table 1.** Material parameters of hyperelastic model for the natural rubber, artery, and thermoplastic elastomer.

	$A_1$ (MPa)	$B_1$ (MPa)	$m_1$	$n_1$	$\alpha_1$	$\beta_1$	RE (%)
Natural rubber	1.996	0.000245	1.348	0.492	0.624	2.083	0.35
Artery	-0.359	16.068	857.23	3860.3	0.235	0.0797	7.8
Artery	40.89	0.0383	0.0012	0.0022	0.9768	0.277	2.78

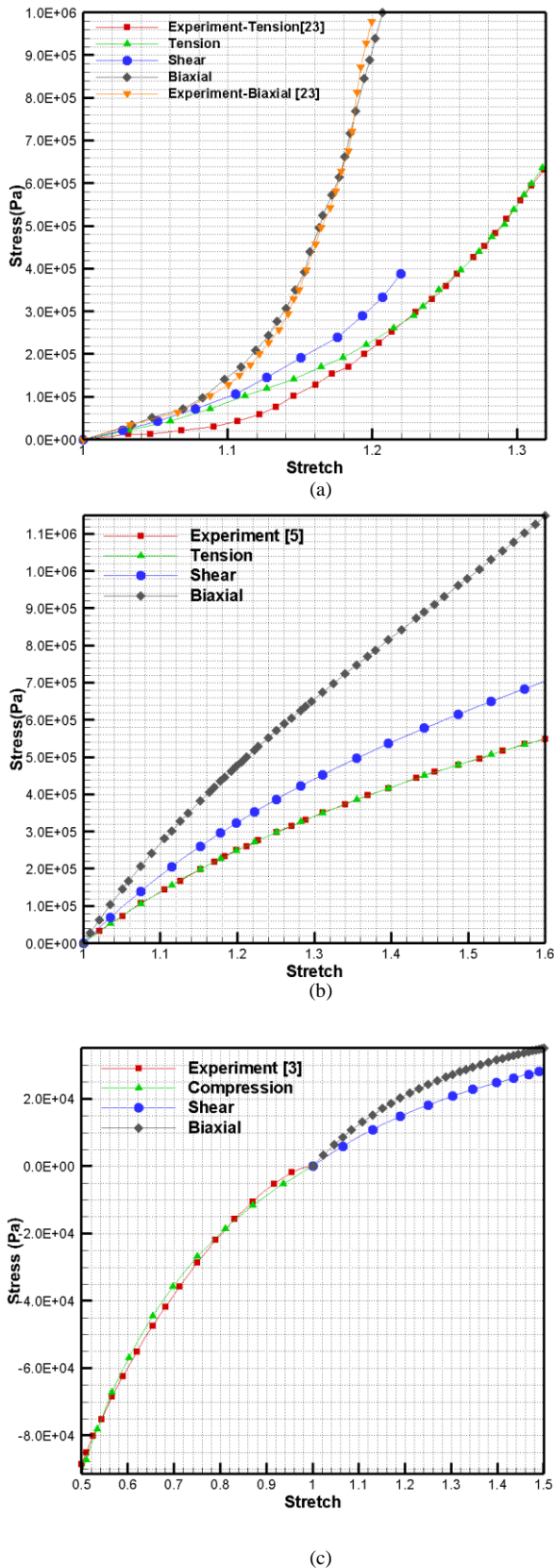


**Figure 1.** Comparison of the experimental [3, 5, 23] and theoretical results of: (a) artery, (b) natural rubber, and (c) thermoplastic elastomer (TPE).

As can be seen from figure 1, the exponential based strain energy function predicted a stable material behavior for basic loading states and a good correlation with the experimental data could be observed. In addition, it has been noticed by Ogden et al that a hyperelastic model should fit uniaxial, equi-biaxial, and pure shear loadings if experimental data are available in these loading

conditions [9]. When there is no experimental data for some loading cases, a model should at least represents a stable behavior (material stability). Both the good fitting and stable material behavior can be seen in figure 1 for various materials. By finding the material constants and ensuring the stable material behavior for different loading modes, in the next subsections simulation of different case studies was investigated using the modified and unmodified exponential based hyperelastic strain energy function.

#### 4.2. Simple tension of the natural rubber

The mechanical behavior of the natural rubber under uniaxial tension was evaluated using the experimental data obtained from Li et al [5]. The same sample as that employed by Li et al was used for simulation, but to reduce the computational time and increase the finite element numerical stability, one eighth of the specimen with the dimensions of  $75 \times 12 \times 1 \text{ mm}^3$  was prepared. According to figure 2, the front edge of the specimen was stretched 39 mm in the z-axis direction. Moreover, symmetrical boundary conditions were assigned to some surfaces as it could be observed from figure 2. The brick elements with reduced integration and enhanced hourglass control were used for simulation.

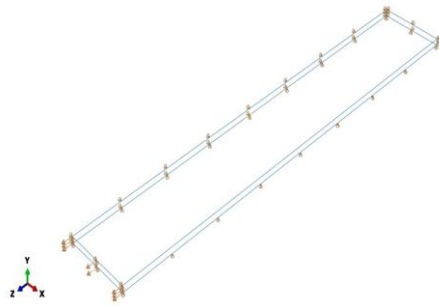


**Figure 2.** Geometry and boundary conditions of natural rubber specimen.

According to figure 1, it is clear that the exponential based hyperelastic strain energy could describe the mechanical behavior appropriately. So, the tension test was simulated using the modified and unmodified formulations. The stress distribution contours are presented in figure 3.

By comparing Figs. 3a and 3b, a different stress distribution could be observed. To obtain the simulated stress-strain curves, the nodal reaction forces of the stretched edge in figure 2 were summed and divided to the initial surface area ( $12 \times 1 \text{ mm}^2$ ) to obtain the average nominal stress (Lagrangian stress) during the simulation. Moreover, to evaluate the engineering strain, the elongation of the long edge was divided to the initial length (75 mm). The stress-strain curves of the modified formulation, the unmodified formulation, and the experimental one can be seen in figure 4.

According to figure 4, it is clear that in the same simulation conditions, by eliminating the ISV term (Eq. 8), the experimental data could be predicted more accurately. Also, the run time required for the unmodified formulation was about 10 times of that needed the modified formulation; this was due to the smaller stable time increment required for the unmodified formulation. That is to say, the numerical stability of the modified formulation was greater than that of the unmodified one, because the existence of the initial pseudo stress increased the stiffness of the material spuriously and therefore, the stable time increment was reduced.

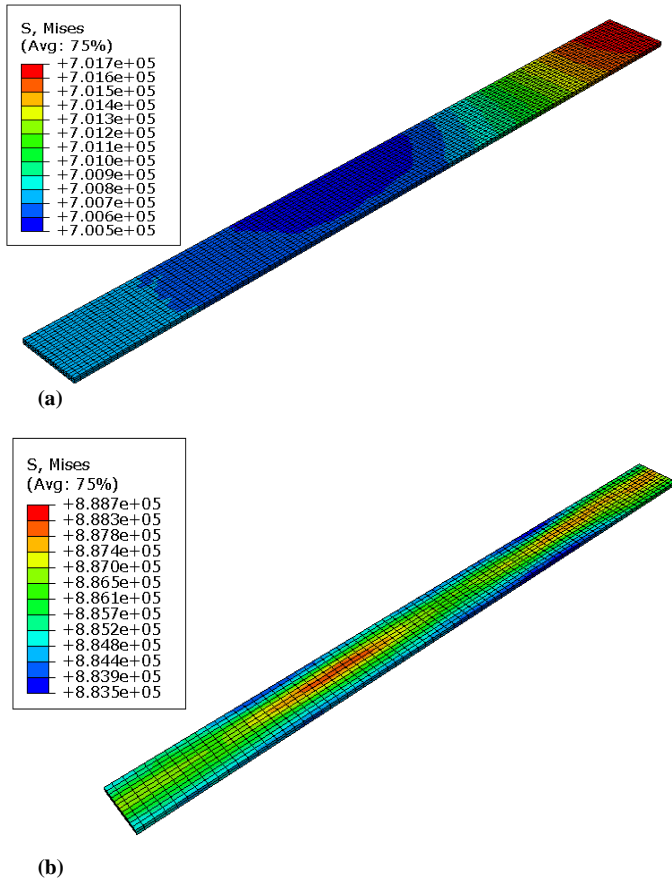


Figure 3. Von- Mises stress (Pa) distribution of natural rubber: (a) modified and (b) unmodified model

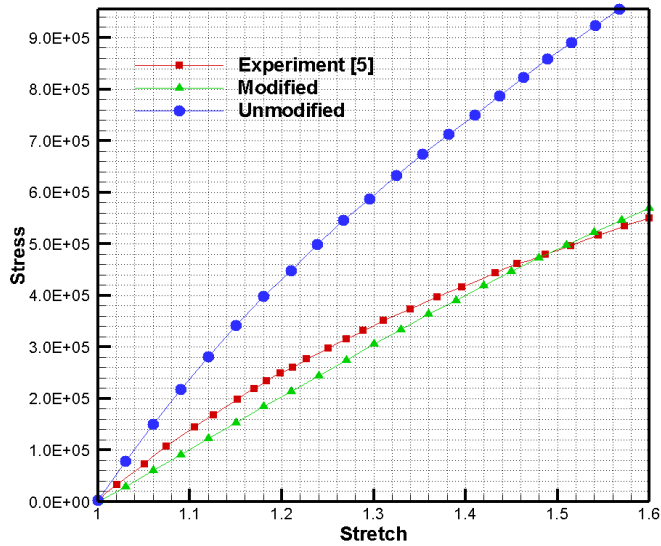


Figure 4. Comparison of the FE results and experimental data of natural rubber [5].

#### 4.3. Compression of thermoplastic elastomer

Uniaxial compression of the thermoplastic elastomer was investigated using both modified and unmodified formulations. One eighth of the specimen with the diameter of 6.35 mm and the height of 3.175 mm was prepared and the symmetrical boundary conditions were assigned to the sides and bottom surfaces, as can be seen in figure 5. A rigid punch was considered to apply the compressive load. The friction coefficient was considered as 0.1

between punch and the deformable specimen. The same element type as the tension test was used for simulation.

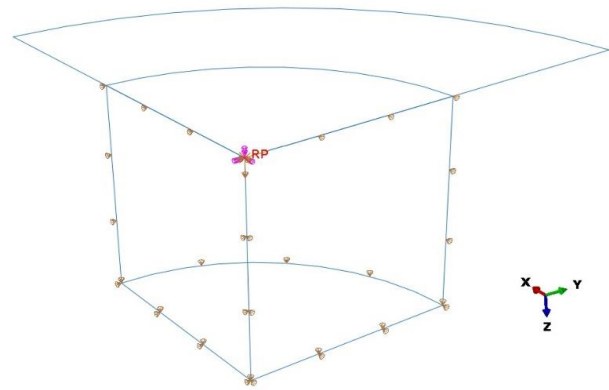


Figure 5. Geometry and boundary conditions of thermoplastic elastomer specimen and punch.

The results of the modified and unmodified models simulation could be observed in figure 6. The simulated stress-strain curves of the modified and unmodified formulations and the experimental stress-strain curve have been plotted in figure 7. According to figure 7, it could be understood that the modified hyperelastic model displayed an appropriate correlation with the experimental results. By comparing Figs. 4 and 7 it could be seen in the small deformation regime (<10% strain) both modified and unmodified models represented nearly the same results; by increasing deformation the difference was enhanced. According to table 1 and Eq. 6, the ISV for rubber was about 1.68 MPa and for the thermoplastic elastomer, it was about 0.05 MPa. Comparing Figs. 4 and 7 and considering the ISV values revealed that when the ISV was increased the difference between the modified and unmodified results was also increased.

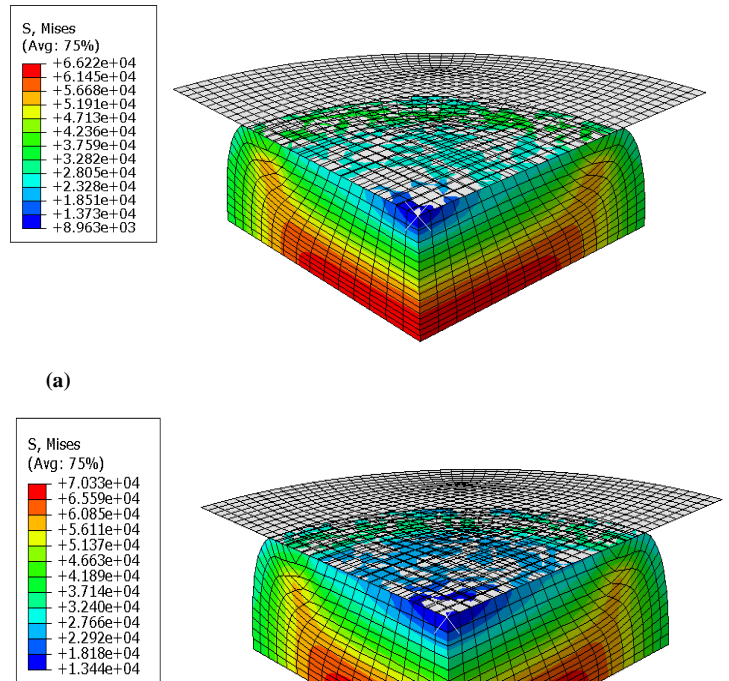


Figure 6. Von-Mises stress (Pa) distribution of thermoplastic elastomer: (a) modified and (b) unmodified models.

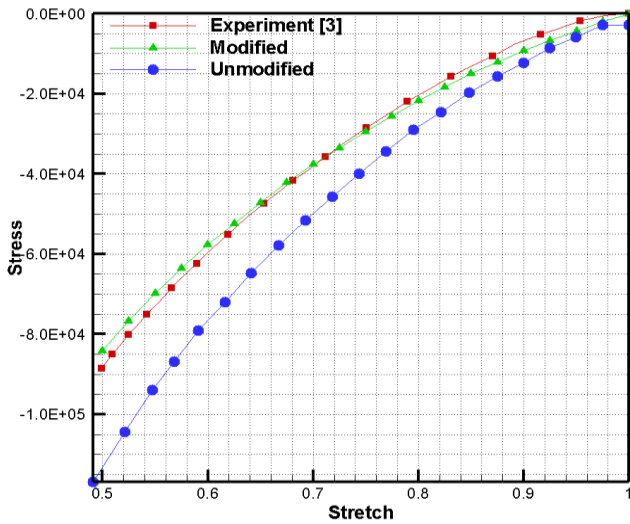


Figure 7. Comparison of the simulation results and experimental data of thermoplastic elastomer [3].

4.4. Stent deployment in the atherosclerosis artery

In recent years, the coronary artery diseases have been identified as the main cause of death after accident. In this section, stent insertion in the human atherosclerosis artery was studied using exponential based hyperelastic equations. The assembled geometry of the model and dimensions of components could be seen in figure 8 and table 2, respectively. It should be noted that although some studies have consider the artery as an anisotropic material, here to represent the modification effect and to compare the results with the reference [26], the artery was considered as isotropic.

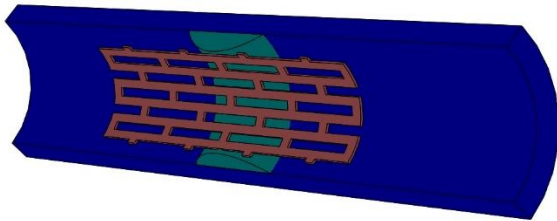


Figure 8. Geometry of artery, stent, and plaque for stent deployment model.

Table 2. Geometrical dimensions of stent deployment model.

	Artery	Stent	Plaque
Length (mm)	20	10	3
Inner diameter (mm)	4	2.9	3
Thickness (mm)	0.5	0.05	0.5

As mentioned previously, in order to reduce the run time and increase the numerical stability, the one eighth model was considered due to the symmetry of geometry. Therefore, symmetric boundary conditions were applied to the left, bottom, and upper edges of the artery, and for the bottom and upper edges of the stent. Similar to the study conducted by Imani et al and Eshghi et al [26, 27], two loading steps were supposed. In the first step, a pressure of 13.3 kPa was applied to the plaque and

the internal wall of the artery for realistic modeling. In the second step, with the preservation of the previous load step, the pressure of 0.4 MPa was applied to the inner wall of the stent to consider the balloon pressure [20, 34, 35]. The stent was considered as the elastic-plastic material with nonlinear hardening (figure 9). In addition, the mechanical property of the plaque was taken into account the 5-term Mooney-Rivlin hyperelastic model [26], and the material coefficients were demonstrated, as shown in table 3.

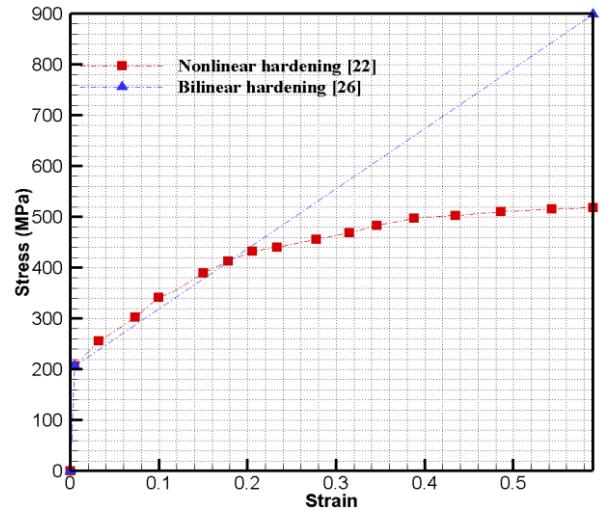
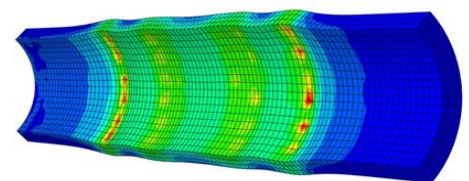
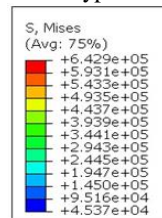


Figure 9. Comparison of nonlinear and bilinear plastic behavior of stent [22, 26].

Table 3. Material parameters of 5-terms Mooney-Rivlin model for plaque [26].

	C <sub>10</sub> (MPa)	C <sub>01</sub> (MPa)	C <sub>20</sub> (MPa)	C <sub>11</sub> (MPa)	C <sub>30</sub> (MPa)
Plaque	-0.495	0.506	1.193	3.637	4.737

Figure 10 illustrates the von Mises stress contour of the human atherosclerosis artery for stent implantation using different hyperelastic constitutive models. As can be seen, the unmodified model predicted stresses more than the modified model, and this could increase the restenosis possibility [26, 36]. In addition, more non-uniformity could be observed in the stress contour of the unmodified formulation. Moreover, comparison of the results of the modified and the 5-term Mooney-Rivlin models showed a significant discrepancy through stent insertion due to the material instability of the equi-biaxial loading of the 5-term Mooney-Rivlin hyperelastic model [26, 27].



(a)

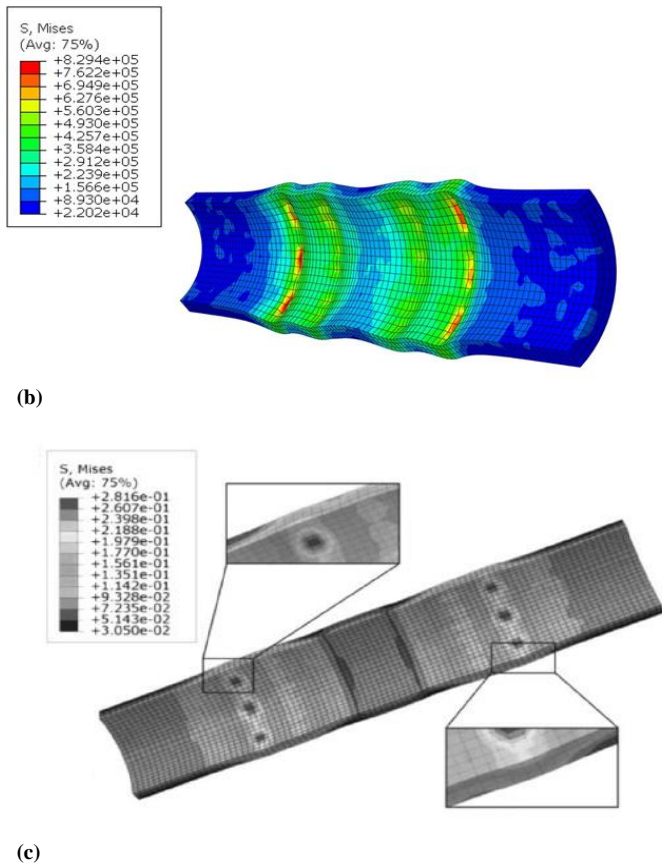


Figure 10. Stress distribution in artery using: (a) modified (Pa), (b) unmodified (Pa), and (c) Mooney-Rivlin (MPa) [26] models.

## 5. Conclusion

In this paper, the exponential based hyperelastic model was modified by eliminating the pseudo initial stresses in the undeformed configuration. Firstly, the exponential based strain energy function was checked by several experimental data (such as the uniaxial compression of the thermoplastic elastomer, the uniaxial tension of the natural rubber, and the uniaxial and equibiaxial tension of the artery) and the best material coefficients were determined. The fitting results indicated that the model captured several experimental data appropriately. In order to verify the modification procedure in the finite element modeling, the VUMAT user subroutines (modified and unmodified states) were provided in the corotational configuration. By using the VUMAT user subroutine, the uniaxial tension of the natural rubber and compression of the thermoplastic elastomer were simulated. The simulation results showed that the modified constitutive model had stability and a good correlation with the experimental data. Finally, implantation of the stent in the atherosclerosis artery was investigated. The results also indicated more acceptable stress ranges and a uniform distribution could be predicted in the artery and stent by using the modified model.

## Acknowledgments

The authors would like to appreciate K. N. Toosi University of Technology, Tehran, Iran, for the financial support and research facilities used in this work.

## References

- [1] A. F. Bower, 2009, *Applied mechanics of solids*, CRC press.
- [2] M. Sasso, G. Palmieri, G. Chiappini, D. Amodio, Characterization of hyperelastic rubber-like materials by biaxial and uniaxial stretching tests based on optical methods, *Polymer Testing*, Vol. 27, No. 8, pp. 995-1004, 2008.
- [3] D. T. Casem, A. K. Dwivedi, R. A. Mrozek, J. L. Lenhart, Compression response of a thermoplastic elastomer gel tissue surrogate over a range of strain-rates, *International Journal of Solids and Structures*, Vol. 51, No. 11, pp. 2037-2046, 2014.
- [4] L. Li, S. Ruan, L. Zeng, Mechanical properties and constitutive equations of concrete containing a low volume of tire rubber particles, *Construction and Building Materials*, Vol. 70, pp. 291-308, 2014.
- [5] X. Li, T. Bai, Z. Li, L. Liu, Influence of the temperature on the hyper-elastic mechanical behavior of carbon black filled natural rubbers, *Mechanics of Materials*, Vol. 95, pp. 136-145, 2016.
- [6] O. A. Shergold, N. A. Fleck, D. Radford, The uniaxial stress versus strain response of pig skin and silicone rubber at low and high strain rates, *International Journal of Impact Engineering*, Vol. 32, No. 9, pp. 1384-1402, 2006.
- [7] T. Beda, Y. Chevalier, Hybrid continuum model for large elastic deformation of rubber, *Journal of applied physics*, Vol. 94, No. 4, pp. 2701-2706, 2003.
- [8] T. Beda, An approach for hyperelastic model-building and parameters estimation a review of constitutive models, *European Polymer Journal*, Vol. 50, pp. 97-108, 2014.
- [9] R. Ogden, G. Saccomandi, I. Sgura, Fitting hyperelastic models to experimental data, *Computational Mechanics*, Vol. 34, No. 6, pp. 484-502, 2004.
- [10] K. Terada, J. Kato, N. Hirayama, T. Inugai, K. Yamamoto, A method of two-scale analysis with micro-macro decoupling scheme: application to hyperelastic composite materials, *Computational Mechanics*, Vol. 52, No. 5, pp. 1199-1219, 2013.
- [11] A. Gendy, A. Saleeb, Nonlinear material parameter estimation for characterizing hyper elastic large strain models, *Computational mechanics*, Vol. 25, No. 1, pp. 66-77, 2000.
- [12] A. Drozdov, Constitutive equations in finite elasticity of rubbers, *International Journal of Solids and Structures*, Vol. 44, No. 1, pp. 272-297, 2007.
- [13] H. Darijani, R. Naghdabadi, M. Kargarnovin, Hyperelastic materials modelling using a strain measure consistent with the strain energy postulates, *Proceedings of the Institution of Mechanical Engineers, Part C: Journal of Mechanical Engineering Science*, Vol. 224, No. 3, pp. 591-602, 2010.
- [14] H. Darijani, R. Naghdabadi, Hyperelastic materials behavior modeling using consistent strain energy density functions, *Acta mechanica*, Vol. 213, No. 3, pp. 235-254, 2010.

- [15] M. Mansouri, H. Darijani, Constitutive modeling of isotropic hyperelastic materials in an exponential framework using a self-contained approach, *International Journal of Solids and Structures*, Vol. 51, No. 25, pp. 4316-4326, 2014.
- [16] B. Fereidoonzhad, R. Naghdabadi, J. Arghavani, A hyperelastic constitutive model for fiber-reinforced rubber-like materials, *International Journal of Engineering Science*, Vol. 71, pp. 36-44, 2013.
- [17] J. H. Smith, J. J. García, Constitutive modeling of brain tissue using Ogden-type strain energy functions, in *Proceeding of*, 2140-2147.
- [18] M. Hosseinzadeh, M. Ghoreishi, K. Narooei, Investigation of hyperelastic models for nonlinear elastic behavior of demineralized and deproteinized bovine cortical femur bone, *Journal of the mechanical behavior of biomedical materials*, Vol. 59, pp. 393-403, 2016.
- [19] N. Elyasi, K. K. Taheri, K. Narooei, A. K. Taheri, A study of hyperelastic models for predicting the mechanical behavior of extensor apparatus, *Biomechanics and modeling in mechanobiology*, Vol. 16, No. 3, pp. 1077-1093, 2017.
- [20] W.-Q. Wang, D.-K. Liang, D.-Z. Yang, M. Qi, Analysis of the transient expansion behavior and design optimization of coronary stents by finite element method, *Journal of Biomechanics*, Vol. 39, No. 1, pp. 21-32, 2006.
- [21] H. Zahedmanesh, C. Lally, Determination of the influence of stent strut thickness using the finite element method: implications for vascular injury and in-stent restenosis, *Medical & biological engineering & computing*, Vol. 47, No. 4, pp. 385, 2009.
- [22] F. AURICCHIO\*, M. Di Loreto, E. Sacco, Finite-element analysis of a stenotic artery revascularization through a stent insertion, *Computer Methods in Biomechanics and Biomedical Engineering*, Vol. 4, No. 3, pp. 249-263, 2001.
- [23] P. Prendergast, C. Lally, S. Daly, A. Reid, T. Lee, D. Quinn, F. Dolan, Analysis of prolapse in cardiovascular stents: a constitutive equation for vascular tissue and finite-element modelling, *Journal of biomechanical engineering*, Vol. 125, No. 5, pp. 692-699, 2003.
- [24] A. Karimi, M. Navidbakhsh, M. Alizadeh, A. Shojaei, A comparative study on the mechanical properties of the umbilical vein and umbilical artery under uniaxial loading, *Artery Research*, Vol. 8, No. 2, pp. 51-56, 2014.
- [25] G. A. Holzapfel, G. Sommer, C. T. Gasser, P. Regitnig, Determination of layer-specific mechanical properties of human coronary arteries with nonatherosclerotic intimal thickening and related constitutive modeling, *American Journal of Physiology-Heart and Circulatory Physiology*, Vol. 289, No. 5, pp. H2048-H2058, 2005.
- [26] M. Imani, A. M. Goudarzi, D. D. Ganji, A. L. Aghili, The comprehensive finite element model for stenting: the influence of stent design on the outcome after coronary stent placement, *Journal of Theoretical and Applied Mechanics*, Vol. 51, No. 3, pp. 639-648, 2013.
- [27] N. Eshghi, M. Hojjati, M. Imani, A. Goudarzi, Finite element analysis of mechanical behaviors of coronary stent, *Procedia Engineering*, Vol. 10, pp. 3056-3061, 2011.
- [28] R. S. Rivlin, D. Saunders, Large elastic deformations of isotropic materials. VII. Experiments on the deformation of rubber, *Philosophical Transactions of the Royal Society of London A: Mathematical, Physical and Engineering Sciences*, Vol. 243, No. 865, pp. 251-288, 1951.
- [29] R. W. Ogden, 1997, *Non-linear elastic deformations*, Courier Corporation,
- [30] W. M. Lai, D. H. Rubin, E. Krempl, D. Rubin, 2009, *Introduction to continuum mechanics*, Butterworth-Heinemann,
- [31] T. Belytschko, W. K. Liu, B. Moran, K. Elkhodary, 2013, *Nonlinear finite elements for continua and structures*, John Wiley & sons,
- [32] R. Ogden, Large deformation isotropic elasticity-on the correlation of theory and experiment for incompressible rubberlike solids, in *Proceeding of*, The Royal Society, pp. 565-584.
- [33] A. F. M. Arif, T. Pervez, M. P. Mughal, Performance of a finite element procedure for hyperelastic-viscoplastic large deformation problems, *Finite elements in analysis and design*, Vol. 34, No. 1, pp. 89-112, 2000.
- [34] F. Etave, G. Finet, M. Boivin, J.-C. Boyer, G. Rioufol, G. Thollet, Mechanical properties of coronary stents determined by using finite element analysis, *Journal of Biomechanics*, Vol. 34, No. 8, pp. 1065-1075, 2001.
- [35] F. Migliavacca, L. Petrini, V. Montanari, I. Quagliana, F. Auricchio, G. Dubini, A predictive study of the mechanical behaviour of coronary stents by computer modelling, *Medical engineering & physics*, Vol. 27, No. 1, pp. 13-18, 2005.
- [36] L. Gu, S. Zhao, A. K. Muttyam, J. M. Hammel, The relation between the arterial stress and restenosis rate after coronary stenting, *Journal of Medical Devices*, Vol. 4, No. 3, pp. 031005, 2010.